

## Flux-difference splitting-based upwind compact schemes for the incompressible Navier–Stokes equations

Abdullah Shah<sup>1,2</sup> and Li Yuan<sup>1,\*</sup>,<sup>†</sup>

<sup>1</sup>*LSEC, Institute of Computational Mathematics and Scientific/Engineering Computing, Academy of Mathematics and Systems Science, Chinese Academy of Sciences, Beijing 100190, People's Republic of China*

<sup>2</sup>*Department of Mathematics, COMSAT Institute of Information Technology, Islamabad, Pakistan*

### SUMMARY

Third-order and fifth-order upwind compact finite difference schemes based on flux-difference splitting are proposed for solving the incompressible Navier–Stokes equations in conjunction with the artificial compressibility (AC) method. Since the governing equations in the AC method are hyperbolic, flux-difference splitting (FDS) originally developed for the compressible Euler equations can be used. In the present upwind compact schemes, the split derivatives for the convective terms at grid points are linked to the differences of split fluxes between neighboring grid points, and these differences are computed by using FDS. The viscous terms are approximated with a sixth-order central compact scheme. Comparisons with 2D benchmark solutions demonstrate that the present compact schemes are simple, efficient, and high-order accurate. Copyright © 2008 John Wiley & Sons, Ltd.

Received 15 November 2007; Revised 29 July 2008; Accepted 10 October 2008

**KEY WORDS:** upwind compact difference; flux-difference splitting; incompressible Navier–Stokes equation; artificial compressibility; backward facing step; lid-driven cavity flow

### 1. INTRODUCTION

The incompressible Navier–Stokes equations (INSE) are mathematical basis for a wide spectrum of fluid flow problems. A difficulty in solving the INSE numerically is the lack of a time-derivative term in the continuity equation, which limits straightforward applications of time-marching numerical methods. Most numerical methods for the INSE require solving pressure or pressure-correction Poisson equation, which serves to satisfy the continuity equation. A representative of these methods

---

\*Correspondence to: Li Yuan, Institute of Computational Mathematics, No. 55 Zhong Guan Cun East Road, Beijing 100190, People's Republic of China.

<sup>†</sup>E-mail: lyuan@lsec.cc.ac.cn

Contract/grant sponsor: Natural Science Foundation of China; contract/grant numbers: G10531080, G10729101

Contract/grant sponsor: State Key Program for Developing Basic Sciences; contract/grant number: 2005CB321703

is the projection method [1], which is very efficient for solving unsteady problems. However, for steady problems, it is desirable to use other cost-effective methods like the artificial compressibility (AC) method [2], which avoids solution of the pressure Poisson equation. The main advantage of the AC method is that it changes the governing equations into hyperbolic–parabolic equations by introducing a pseudo-time derivative of pressure into the continuity equation, hence subsequent discretization and solution methods can be borrowed from efficient schemes developed for compressible flows.

The AC method has been extensively developed for solving steady-state and time-dependent flow problems in the past four decades. Rogers and Kwak [3, 4], among others [5–9], have implemented the AC method in conjunction with various discretization schemes and solution algorithms, most of which are borrowed from compressible flow solvers. Particularly, Rogers and Kwak [3] have developed a third-order upwind finite difference scheme for the convective terms based on flux-difference splitting (FDS). Their scheme was widely used in various applications. However, our experience has shown that this scheme was a bit too diffusive for vortical flows. Meanwhile, some other popular numerical schemes like MUSCL and WENO schemes were also implemented in conjunction with the AC method [7–9]. However, the MUSCL scheme for a nonlinear equation has at most second-order accuracy, and the WENO scheme is computationally expensive in spite of being formally high-order accurate. Therefore, more accurate and economical discretization schemes are desired.

In the development of appropriate discretization schemes for high accuracy simulation of complex flows, compact finite difference schemes represent an attractive choice because for the same number of points in the stencil, they yield higher accuracy and better spectral resolution than their non-compact counterparts [10, 11]. Compact schemes have two categories: central and upwind. When applied to the convective terms, the upwind compact schemes with dissipative properties are more stable and more economical in computation than the central compact schemes, as they do not need extra filtering as needed by the central compact schemes for suppressing numerical instabilities [12]. Fu *et al.* [13], Fu and Ma [14], and others [15, 16] have developed some upwind compact schemes for compressible flows. These upwind, dissipative schemes can in principle prevent non-physical oscillations in flows without discontinuities, therefore, they are worthy to be applied to incompressible flows.

The objective of the present study is to extend the third-order and the fifth-order upwind compact schemes developed by Fu *et al.* [13], Fu and Ma [14] to discretization of the convective terms of the INSE in conjunction with the AC approach. The peculiarity of the two upwind compact schemes lies in that their implicit parts involve only two points while most other versions of upwind compact schemes involve more than two [17]. This will reduce a reasonable amount of computational costs.

In this paper, implementation of the third-order and the fifth-order upwind compact finite difference schemes for discretizing the convective terms are presented in detail. The explicit parts of the compact schemes are computed according to Rogers and Kwak's implementation of FDS in their non-compact upwind schemes [3, 4], while the implicit parts of the compact schemes remain the same bi-diagonal equations as in the original upwind compact schemes [13, 14]. The boundary schemes are also given. To show the orders of accuracy for the two upwind compact schemes, a sixth-order central compact scheme is employed for the viscous terms. This paper is not concerned with the solution algorithm, thus the traditional Beam–Warming approximate factorization scheme is employed. The robustness and accuracy of the present compact schemes are verified through several 2D benchmark problems.

The remainder of the paper is organized as follows. In Section 2, formulation for the AC method is briefly outlined. Section 3 presents the spatial discretization including the upwind compact schemes for the convective terms and the central compact scheme for the viscous terms. Section 4 describes the solution algorithm for the discretized equations. The computed results for several 2D flow problems are presented in Section 5. Finally, the conclusions are given in Section 6.

## 2. GOVERNING EQUATIONS

The governing equations are the 2D non-dimensional INSE in Cartesian coordinates  $(x, y)$  with the AC term added to the continuity equation [4]:

$$\mathbf{Q}_\tau + (\mathbf{E} - \mathbf{E}_v)_x + (\mathbf{F} - \mathbf{F}_v)_y = \mathbf{0} \quad (1)$$

where

$$\mathbf{Q} = \begin{pmatrix} p \\ u \\ v \end{pmatrix}, \quad \mathbf{E} = \begin{pmatrix} \beta u \\ u^2 + p \\ uv \end{pmatrix}, \quad \mathbf{F} = \begin{pmatrix} \beta v \\ uv \\ v^2 + p \end{pmatrix}, \quad \mathbf{E}_v = \frac{1}{Re} \begin{pmatrix} 0 \\ u_x \\ v_x \end{pmatrix}, \quad \mathbf{F}_v = \frac{1}{Re} \begin{pmatrix} 0 \\ u_y \\ v_y \end{pmatrix}$$

Here  $\mathbf{Q}$  is the solution vector,  $\tau$  is the pseudo-time,  $u$  and  $v$  are velocity components,  $p$  is the pressure,  $Re$  is the Reynolds number, and  $\beta$  is the AC factor. Subscripts denote partial derivatives. Because of the addition of the AC term, the resulting equations become hyperbolic type in time, with the Jacobian matrices  $\mathbf{A}$  and  $\mathbf{B}$  for the inviscid flux vectors given by

$$\mathbf{A} = \frac{\partial \mathbf{E}}{\partial \mathbf{Q}} = \begin{bmatrix} 0 & \beta & 0 \\ 1 & 2u & 0 \\ 0 & v & u \end{bmatrix}, \quad \mathbf{B} = \frac{\partial \mathbf{F}}{\partial \mathbf{Q}} = \begin{bmatrix} 0 & 0 & \beta \\ 0 & v & u \\ 1 & 0 & 2v \end{bmatrix} \quad (2)$$

The Jacobian matrices  $\mathbf{A}_v$  and  $\mathbf{B}_v$  of the viscous flux vectors, which will appear in an implicit method are

$$\mathbf{A}_v = \frac{\partial \mathbf{E}_v}{\partial \mathbf{Q}} = \frac{\mathbf{I}_m}{Re} \frac{\partial}{\partial x}, \quad \mathbf{B}_v = \frac{\partial \mathbf{F}_v}{\partial \mathbf{Q}} = \frac{\mathbf{I}_m}{Re} \frac{\partial}{\partial y} \quad \text{with } \mathbf{I}_m = \begin{bmatrix} 0 & 0 & 0 \\ 0 & 1 & 0 \\ 0 & 0 & 1 \end{bmatrix} \quad (3)$$

The matrix  $\mathbf{I}_m$  is a modified identity matrix. It is possible to diagonalize  $\mathbf{A}$  and  $\mathbf{B}$  as

$$\mathbf{A} = \mathbf{X} \mathbf{\Lambda}_A \mathbf{X}^{-1}, \quad \mathbf{B} = \mathbf{Y} \mathbf{\Lambda}_B \mathbf{Y}^{-1} \quad (4)$$

where diagonal matrices  $\mathbf{\Lambda}_A$  and  $\mathbf{\Lambda}_B$  contain the eigenvalues of matrices  $\mathbf{A}$  and  $\mathbf{B}$ :

$$\text{diag}(\mathbf{\Lambda}_A) = \{u, u + c_1, u - c_1\}, \quad \text{diag}(\mathbf{\Lambda}_B) = \{v, v + c_2, v - c_2\} \quad (5)$$

with  $c_1 = \sqrt{u^2 + \beta}$  and  $c_2 = \sqrt{v^2 + \beta}$  being the pseudo-speeds of sound in  $x$  and  $y$  directions, respectively.  $\mathbf{X}$  and  $\mathbf{Y}$  are matrices of the right eigenvectors, while  $\mathbf{X}^{-1}$  and  $\mathbf{Y}^{-1}$  are matrices of the left eigenvectors, respectively. These matrices are given by

$$\mathbf{X} = \begin{bmatrix} 0 & c_1(c_1 - u) & c_1(c_1 + u) \\ 0 & c_1 & -c_1 \\ 1 & v & v \end{bmatrix}, \quad \mathbf{X}^{-1} = \frac{1}{c_1^2} \begin{bmatrix} -v & -uv & c_1^2 \\ \frac{1}{2} & \frac{1}{2}(c_1 + u) & 0 \\ \frac{1}{2} & -\frac{1}{2}(c_1 - u) & 0 \end{bmatrix}$$

and

$$\mathbf{Y} = \begin{bmatrix} 0 & c_2(c_2 - v) & c_2(c_2 + v) \\ 1 & u & u \\ 0 & c_2 & -c_2 \end{bmatrix}, \quad \mathbf{Y}^{-1} = \frac{1}{c_2^2} \begin{bmatrix} -u & c_2^2 & -uv \\ \frac{1}{2} & 0 & \frac{1}{2}(c_2 + v) \\ \frac{1}{2} & 0 & -\frac{1}{2}(c_2 - v) \end{bmatrix}$$

### 3. SPATIAL DISCRETIZATION SCHEMES

Owing to the hyperbolic nature of system (1), the convective flux, and thus its derivative, can be split into two parts, e.g. in the  $x$  direction,

$$\mathbf{E}_x = (\mathbf{E}^+ + \mathbf{E}^-)_x = \mathbf{E}_x^+ + \mathbf{E}_x^- \tag{6}$$

where  $\mathbf{E}^+$  corresponds to the split flux in the positive  $x$  direction with information being propagated from left to right by positive eigenvalues and  $\mathbf{E}^-$  corresponds to the split flux in the negative  $x$  direction with information being propagated from right to left by negative eigenvalues. To compute the two split derivatives in Equation (6), we use the third-order and the fifth-order upwind compact schemes [13, 14], which are

$$\frac{2}{3}(\mathbf{E}_x^+)_i + \frac{1}{3}(\mathbf{E}_x^+)_{i-1} = \frac{5\delta^-\mathbf{E}_i^+ + \delta^-\mathbf{E}_{i+1}^+}{6\Delta x} + \mathcal{O}(\Delta x^3) \tag{7a}$$

$$\frac{2}{3}(\mathbf{E}_x^-)_i + \frac{1}{3}(\mathbf{E}_x^-)_{i+1} = \frac{5\delta^+\mathbf{E}_i^- + \delta^+\mathbf{E}_{i-1}^-}{6\Delta x} + \mathcal{O}(\Delta x^3) \tag{7b}$$

and

$$\frac{3}{5}(\mathbf{E}_x^+)_i + \frac{2}{5}(\mathbf{E}_x^+)_{i-1} = \frac{-\delta^-\mathbf{E}_{i+2}^+ + 11\delta^-\mathbf{E}_{i+1}^+ + 47\delta^-\mathbf{E}_i^+ + 3\delta^-\mathbf{E}_{i-1}^+}{60\Delta x} + \mathcal{O}(\Delta x^5) \tag{8a}$$

$$\frac{3}{5}(\mathbf{E}_x^-)_i + \frac{2}{5}(\mathbf{E}_x^-)_{i+1} = \frac{-\delta^+\mathbf{E}_{i-2}^- + 11\delta^+\mathbf{E}_{i-1}^- + 47\delta^+\mathbf{E}_i^- + 3\delta^+\mathbf{E}_{i+1}^-}{60\Delta x} + \mathcal{O}(\Delta x^5) \tag{8b}$$

respectively, where  $\delta^+ f_i = f_{i+1} - f_i$ ,  $\delta^- f_i = f_i - f_{i-1}$ , and  $\Delta x$  is the grid spacing of uniform grids used throughout this paper. Equations (7) and (8) are explicitly marched forward and backward to

get all the derivatives once the right-hand side (RHS) and the boundary derivatives are given. The advantages of these upwind compact schemes are: (i) their computational cost is only marginally larger than the non-compact upwind biased schemes of Rogers and Kwak [4], but they have much better resolution properties than their non-compact counterparts; (ii) unlike central compact schemes, they automatically provide odd–even coupling of grid points and numerical dissipation to damp out high-frequency oscillations. The next step is how to evaluate the RHS of Equations (7) and (8).

In References [13, 14], the point-wise  $\mathbf{E}_i^\pm$  in the RHS of Equations (7) and (8) were constructed by using Steger–Warming flux vector splitting for compressible flows. However, Steger–Warming splitting requires that the convective flux be a homogeneous function of the solution vector, which is not the case with incompressible flows. Thus a better option is to use FDS, as previously done for non-compact schemes [3, 4, 6].

Since each term in the RHS of Equations (7) and (8) represents the difference of split fluxes between neighboring points, we can compute them by using FDS [18]

$$\mathbf{E}_{i+1}^\pm - \mathbf{E}_i^\pm \equiv \Delta \mathbf{E}_{i+1/2}^\pm = \mathbf{A}^\pm(\bar{\mathbf{Q}})(\mathbf{Q}_{i+1} - \mathbf{Q}_i) \tag{9}$$

where  $\Delta \mathbf{E}_{i+1/2}^\pm$  is the flux difference across the positive or negative traveling waves. The split Jacobian matrix is calculated by  $\mathbf{A}^\pm(\bar{\mathbf{Q}}) = \mathbf{X} \Lambda_A^\pm \mathbf{X}^{-1}$ , which is evaluated using some intermediate value  $\bar{\mathbf{Q}}$ . The Roe properties [18], which are necessary for a conservative scheme, are satisfied exactly if  $\bar{\mathbf{Q}}$  is taken as the average of the surrounding points for incompressible flows [4, 6], i.e.

$$\bar{\mathbf{Q}} = \frac{1}{2}(\mathbf{Q}_{i+1} + \mathbf{Q}_i) \tag{10}$$

To close the third-order scheme, Equation (7), at interior points, an explicit, dissipative, and third-order one-sided boundary scheme [19] is used at boundary points

$$\begin{aligned} \text{at } i = 1: (\mathbf{E}_x^+)_i &= \frac{-11\mathbf{E}_i^+ + 18\mathbf{E}_{i+1}^+ - 9\mathbf{E}_{i+2}^+ + 2\mathbf{E}_{i+3}^+}{6\Delta x} \\ &= \frac{11\Delta \mathbf{E}_{i+1/2}^+ - 7\Delta \mathbf{E}_{i+3/2}^+ + 2\Delta \mathbf{E}_{i+5/2}^+}{6\Delta x} + \mathcal{O}(\Delta x^3) \end{aligned} \tag{11a}$$

$$\begin{aligned} \text{at } i = N: (\mathbf{E}_x^-)_i &= \frac{11\mathbf{E}_i^- - 18\mathbf{E}_{i-1}^- + 9\mathbf{E}_{i-2}^- - 2\mathbf{E}_{i-3}^-}{6\Delta x} \\ &= \frac{11\Delta \mathbf{E}_{i-1/2}^- - 7\Delta \mathbf{E}_{i-3/2}^- + 2\Delta \mathbf{E}_{i-5/2}^-}{6\Delta x} + \mathcal{O}(\Delta x^3) \end{aligned} \tag{11b}$$

It has been shown in Reference [20] that a boundary scheme of one-order lower accuracy is sufficient to maintain the interior order of accuracy for the global discretization. For the boundary scheme of the fifth-order upwind compact scheme, Equation (8), a fourth-order explicit biased scheme [21] is used at next to boundary points:

$$\begin{aligned} \text{at } i = 2: (\mathbf{E}_x^+)_i &= \frac{-3\mathbf{E}_{i-1}^+ - 10\mathbf{E}_i^+ + 18\mathbf{E}_{i+1}^+ - 6\mathbf{E}_{i+2}^+ + \mathbf{E}_{i+3}^+}{12\Delta x} \\ &= \frac{3\Delta \mathbf{E}_{i-1/2}^+ + 13\Delta \mathbf{E}_{i+1/2}^+ - 5\Delta \mathbf{E}_{i+3/2}^+ + \Delta \mathbf{E}_{i+5/2}^+}{12\Delta x} + \mathcal{O}(\Delta x^4) \end{aligned} \tag{12a}$$

$$\begin{aligned}
 \text{at } i = N - 1: (\mathbf{E}_x^-)_i &= \frac{3\mathbf{E}_{i+1}^- + 10\mathbf{E}_i^- - 18\mathbf{E}_{i-1}^- + 6\mathbf{E}_{i-2}^- - \mathbf{E}_{i-4}^-}{12\Delta x} \leftarrow \boxed{i-3} \\
 &= \frac{3\Delta\mathbf{E}_{i+1/2}^- + 13\Delta\mathbf{E}_{i-1/2}^- - 5\Delta\mathbf{E}_{i-3/2}^- + \Delta\mathbf{E}_{i-5/2}^-}{12\Delta x} + \mathcal{O}(\Delta x^4) \quad (12b)
 \end{aligned}$$

The discretization of the viscous terms is performed with central schemes. The second derivative for the viscous terms in Equation (1) is approximated with a sixth-order symmetric compact scheme due to Collatz [11] at interior points

$$2S_{i-1} + 11S_i + 2S_{i+1} = 12 \frac{u_{i-1} - 2u_i + u_{i+1}}{\Delta x^2} + \frac{3}{4} \frac{u_{i-2} - 2u_i + u_{i+2}}{\Delta x^2}, \quad 3 \leq i \leq N - 2 \quad (13)$$

where  $S_i$  approximates  $(\partial^2 u / \partial x^2)_i$ . To obtain  $S_i$ , a linear system of equations with a tri-diagonal matrix has to be solved. To close the tri-diagonal equations at both ends, we propose a third-order compact boundary scheme at next to boundary points

$$S_i - S_{i+1} = \frac{1}{\Delta x^2} (u_{i-1} - 3u_i + 3u_{i+1} - u_{i+2}), \quad i = 2 \quad (14a)$$

$$S_i - S_{i-1} = \frac{1}{\Delta x^2} (u_{i+1} - 3u_i + 3u_{i-1} - u_{i-2}), \quad i = N - 1 \quad (14b)$$

#### 4. IMPLICIT APPROXIMATE FACTORIZATION METHOD

By applying the backward difference to the pseudo-time derivative in Equation (1), we obtain

$$\frac{\Delta \mathbf{Q}^m}{\Delta \tau} + [(\mathbf{E} - \mathbf{E}_v)_x + (\mathbf{F} - \mathbf{F}_v)_y]^{m+1} = 0 \quad (15)$$

where  $\Delta \mathbf{Q}^m = \mathbf{Q}^{m+1} - \mathbf{Q}^m$ , and  $m$  refers to the pseudo-time level.

Terms at  $m + 1$  pseudo-time level are linearized with respect to  $m$ th level by using Taylor expansion, e.g.

$$\mathbf{E}^{m+1} \approx \mathbf{E}^m + \left( \frac{\partial \mathbf{E}}{\partial \mathbf{Q}} \right)^m (\mathbf{Q}^{m+1} - \mathbf{Q}^m) = \mathbf{E}^m + \mathbf{A}^m \Delta \mathbf{Q}^m \quad (16a)$$

$$(\mathbf{E}_v)^{m+1} \approx (\mathbf{E}_v)^m + \left( \frac{\partial \mathbf{E}_v}{\partial \mathbf{Q}} \right)^m (\mathbf{Q}^{m+1} - \mathbf{Q}^m) = (\mathbf{E}_v)^m + \mathbf{A}_v^m \Delta \mathbf{Q}^m \quad (16b)$$

Thus we obtain the so-called delta form (solution to incremental variables  $\Delta \mathbf{Q}$ )

$$\begin{aligned}
 & \{ \mathbf{I} + \Delta \tau [(\mathbf{A} - \mathbf{A}_v)_x + (\mathbf{B} - \mathbf{B}_v)_y] \}^m \Delta \mathbf{Q}^m \\
 & = -\Delta \tau [(\mathbf{E} - \mathbf{E}_v)_x + (\mathbf{F} - \mathbf{F}_v)_y]^m \\
 & = -\mathbf{R}^m \quad (17)
 \end{aligned}$$

The Beam-Warming approximate factorization scheme [22] can be symbolically written as

$$\mathcal{L} \cdot \Delta \mathbf{Q}^m \approx \mathcal{L}_x \mathcal{L}_y \cdot \Delta \mathbf{Q}^m = -\mathbf{R}^m \quad (18)$$

Remember that high-order compact schemes are used only for the RHS,  $\mathbf{R}^m$ . To obtain block tri-diagonal equations, convective terms on the left-hand side (LHS) of Equation (17) are discretized by the first-order upwind difference and viscous terms by traditional second-order central differences, e.g.

$$\delta_x^+ f_i = \frac{f_{i+1} - f_i}{\Delta x}, \quad \delta_x^- f_i = \frac{f_i - f_{i-1}}{\Delta x} \quad \text{and} \quad \delta_x^2 f_i = \frac{(f_{i+1} - 2f_i + f_{i-1}))}{\Delta x^2}$$

Further on, we obtain the approximate factorization scheme

$$\left[ \mathbf{I} + \Delta\tau \left( \delta_x^- \mathbf{A}^+ + \delta_x^+ \mathbf{A}^- - \frac{\mathbf{I}_m}{Re} \delta_x^2 \right) \right] \left[ \mathbf{I} + \Delta\tau \left( \delta_y^- \mathbf{B}^+ + \delta_y^+ \mathbf{B}^- - \frac{\mathbf{I}_m}{Re} \delta_y^2 \right) \right] \Delta \mathbf{Q}^m = -\mathbf{R}^m \quad (19)$$

which is solved by the alternating-direction implicit method.

To simplify the computation, the split inviscid Jacobian matrix in the LHS of Equation (19) is approximated by

$$\mathbf{A}^\pm = \frac{1}{2} [\mathbf{A} \pm \rho(\mathbf{A}) \mathbf{I}] \quad \text{with} \quad \rho(\mathbf{A}) = \kappa \max[|\lambda(\mathbf{A})|] \quad (20)$$

where  $\lambda(\mathbf{A})$  represents the eigenvalues of the matrix  $\mathbf{A}$ , and  $\kappa$  is a constant that is greater than or equal to unity [4]. In this paper, it is found that  $\kappa=1$  is sufficient for the third-order upwind compact scheme, while  $\kappa \geq 1.2 \sim 1.3$  is necessary for numerical stability of the fifth-order upwind compact scheme.

## 5. NUMERICAL EXAMPLES

In this section, the numerical method developed in Sections 3 and 4 is tested against several benchmark problems. Computational results for pressure-driven flows (namely, the steady plane Poiseuille flow and Couette–Poiseuille flow), the flow over a backward facing step and the lid-driven square cavity flow are presented. Finally, a grid refinement study of a modified cavity flow problem which has an analytical solution for the INSE is conducted to quantify the numerical order of accuracy of the upwind compact schemes.

### 5.1. Pressure-driven flows

The pressure-driven flows include the plane Poiseuille flow and the plane Couette–Poiseuille flow between two parallel plates (e.g. see [23]). Both problems are governed by a reduced INSE for one dependent variable  $u = u(y)$  with different boundary conditions for different cases:

$$\begin{aligned} \Pi + \frac{d^2 u}{dy^2} &= 0 \\ u(0) &= 0 \\ u(1) &= U_{\text{top}} \end{aligned} \quad (21)$$

where  $U_{\text{top}}=0$  represents the plane Poiseuille flow whose exact solution is  $u(y) = \Pi/2(y - y^2)$ ,  $U_{\text{top}}=1$  represents the plane Couette–Poiseuille flow whose exact solution is  $u(y) = \Pi/2(y - y^2) + y$ , and  $\Pi = -\partial \bar{p} / \partial x$  is a dimensionless constant pressure gradient. In our computation, the

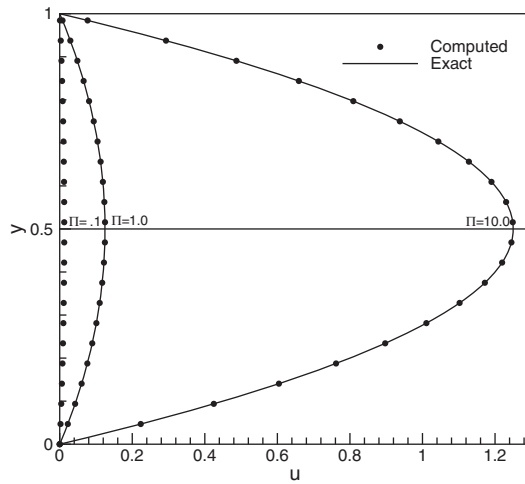


Figure 1. Velocity profiles for the Poiseuille flow.

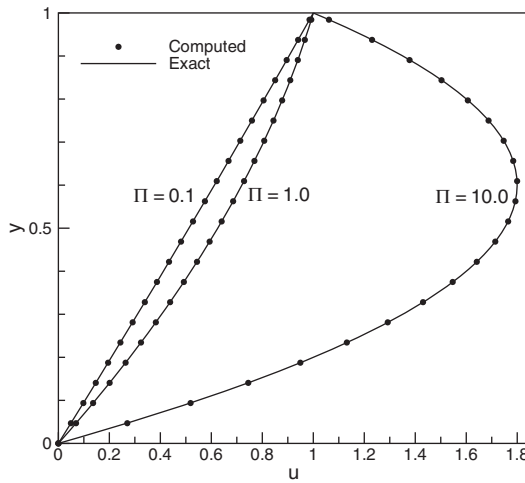


Figure 2. Velocity profiles for the Couette–Poiseuille flow.

computational grid used had  $65 \times 65$  uniform-mesh points, and various values of  $\beta$  and CFL numbers were used. The boundary conditions are: zero normal pressure gradient and no-slip velocity on either plate;  $\Pi$  value at the inlet and zero value at the outlet for the pressure; and zero gradient for the velocity at both the inlet and the outlet. Both third-order and fifth-order upwind compact schemes give nearly identical results. Only results for the third-order scheme are demonstrated in this subsection. Figure 1 shows the computed velocity profiles for three values of  $\Pi$  for the Poiseuille flow, and Figure 2 shows those for the Couette–Poiseuille flow. It can be seen that the

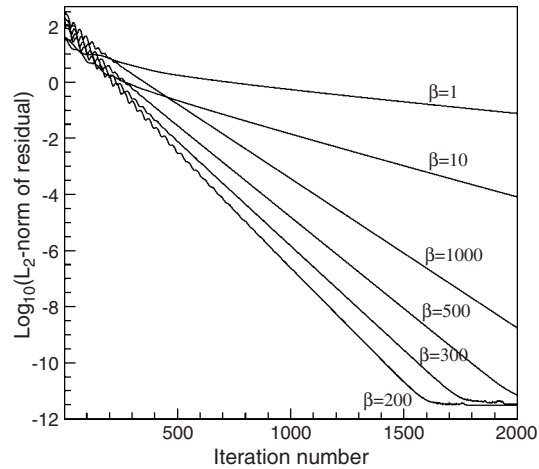


Figure 3. Convergence history for different artificial compressibility factors for the Couette–Poiseuille flow and the same CFL=10.

computational results agree very well with the analytical solutions. In fact, the numerical error is found to be within  $10^{-12}$ , which is close to machine accuracy.

Since the AC method has the drawback that its convergence rate and stability depend on the AC factor  $\beta$ , we have to make a test to get a rule of thumb for choosing  $\beta$ . In this regard, several techniques were available in the literature for choosing an optimal  $\beta$ , see, for instance [24–27]. Particularly, Reference [27] gave a specific lower bound of  $\beta$  to prevent viscous effects from coupling the pseudo-pressure waves, and a crude upper bound for the approximate factorization errors not to spoil the computational accuracy. Between the two bounds existed a wide range of choices. However, in general, the superiority of one choice over another is not known in advance. Figure 3 shows the convergence history for different values of  $\beta$  at the same CFL number. The convergence rate is not monotone with  $\beta$ , and the best rate is achieved for  $\beta=200$ . Figure 4 shows the optimal converge for each value of  $\beta$  at its optimal CFL number. One can see that the convergence rate is not much affected by different values of  $\beta$  in the range of 10–1000 if an optimal CFL number corresponding to each  $\beta$  is chosen. Therefore, it is not necessary to tune  $\beta$  extensively, and a moderate value of  $\beta$ , say 100, generally is fine.

### 5.2. Flow over a backward facing step

Another standard test case commonly employed for validating incompressible flow solvers at moderate Reynolds numbers is the recirculating flow over a backward facing step. Unlike the channel flow in the previous subsection, the challenge in simulating this problem is to handle the recirculation region immediately downstream of the step and for sufficiently high Reynolds numbers the recirculation zone further downstream on the upper wall. Numerical results obtained using a variety of methods were available in the literature, e.g. Kim and Moin [28], Gartling [29], and Rogers and Kwak [4], and experimental results were given by Armaly *et al.* [30].

Consider a channel of width  $h/2$  upstream of the origin, and a length of  $30h$  downstream of the origin, separated by a backward facing step as shown in Figure 5. The flow is assumed to be fully developed as it passes the inlet at  $x=0$  and has an average velocity  $U_{ave}$ . The top and bottom

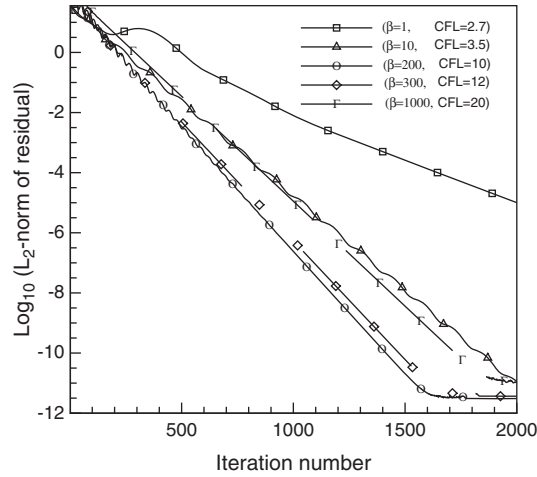


Figure 4. Convergence history for different values of  $\beta$  at optimal CFL numbers.

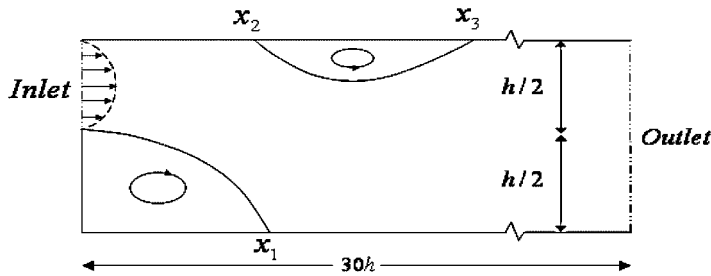


Figure 5. Geometry of the backward facing step flow problem and the recirculation zones.

boundaries are stationary walls and non-slip boundary conditions are applied for the velocity while the pressure is extrapolated from the interior. The step face located at  $-0.5 < y < 0$  is also stationary wall. The velocity components at the inlet are given by

$$u = 12y(1 - 2y), \quad v = 0 \tag{22}$$

and the pressure at the inlet is extrapolated, while the outflow boundary consists of zero normal derivative for velocity and zero pressure. The location of the outflow is sufficiently far downstream of the step so as not to affect the position of recirculation zones. The computational grid used has  $101 \times 301$  grid points. Other parameters are  $\beta = 100$ , and  $\text{CFL} = 10$ . The results of the third-order scheme are shown for this problem.

Figure 6(a)–(c) shows comparison of computed separation and reattachment positions  $x_1, x_2, x_3$  (see Figure 5), respectively with experimental and other numerical results for different Reynolds numbers. Good agreement can be seen between the present results and available numerical results especially those of Rogers *et al.* [4]. For  $Re \geq 400$ , the deviation of the experimental results from the computational ones, particularly for  $x_2$ , may be due to possible 3D effects in the experiment.

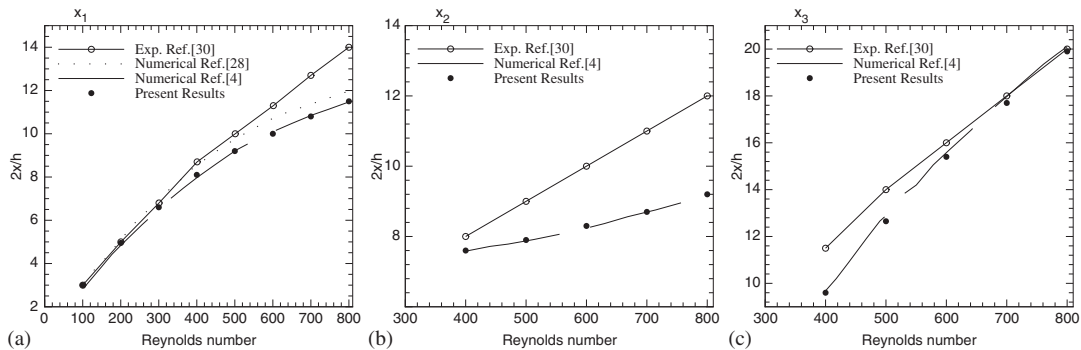


Figure 6. Comparison of non-dimensional reattachment and separation lengths.

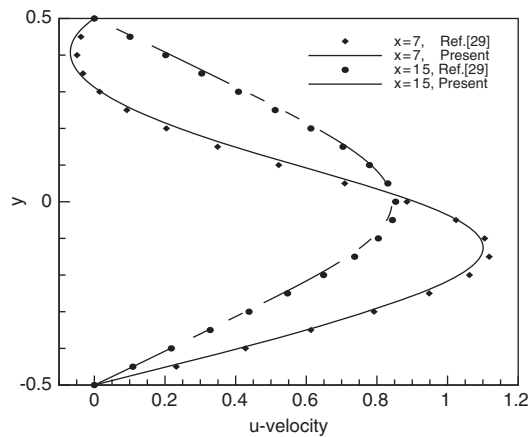


Figure 7. Horizontal velocity profiles along the height of the channel at  $Re=800$ .

In Figure 7,  $u$ -velocity profiles along the channel height at  $x=7$  and 15 are compared with the computational results of Gartling [29], and it can be seen that both match well. Finally, the streamline contours in Figure 8 clearly show the evolution in the position of the separation and reattachment with the Reynolds number.

### 5.3. Lid-driven cavity flow

Next, the well-known 2D lid-driven square cavity flow problem is used to test our scheme. The flow is driven by the translation of the top lid. The resulting flow is of great scientific interest because it displays rich fluid mechanical phenomena in the simplest of geometrical settings. Thus, vortices, non-uniqueness, transition, and turbulence all occur naturally and can be studied in the same closed geometry [31]. Top moving wall generates vorticity that diffuses into the cavity and this diffusion becomes the driven mechanism of the flow. For high Reynolds numbers, several secondary and tertiary vortices begin to appear, whose characteristics depend on the Reynolds number. Since for  $5000 < Re < 15000$ , the flow becomes time periodic and for  $15000 \leq Re \leq 20000$ ,

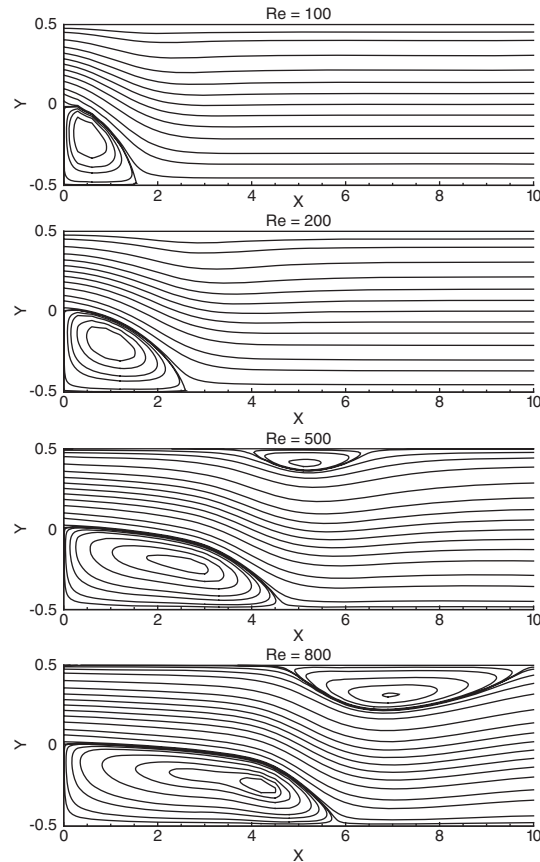


Figure 8. Flow over a backward facing step: streamlines at different Reynolds numbers.

it becomes chaotic [32], we only computed several Reynolds numbers ranging from 100 to 5000 for obtaining stationary solutions. The AC factor  $\beta$  is set to 100. Only the result computed with the third-order scheme is given for this problem.

In Figure 9, the streamline contours show the ability of the present third-order scheme to predict the primary, secondary and particularly, tertiary vortices at higher Reynolds numbers. The computed streamline patterns are similar to those of [32, 33].

Figure 10 shows comparison of the  $u$ - and  $v$ -velocity components for  $Re=1000$  on the lines given by  $x=0.5$  and  $y=0.5$ , respectively, with the calculations of Ghia *et al.* [33]. An excellent agreement has been observed between both results.

#### 5.4. Modified cavity flow

A recirculating cavity flow problem in the domain  $(0 \leq (x, y) \leq 1)$  driven by combined shear and body forces has an exact solution for the INSE [34, 35] and it is used here to compare the numerical solution with the exact solution so as to verify the order of accuracy of the upwind compact schemes on uniform grids. To exclude the influence of implementing the pressure boundary condition on

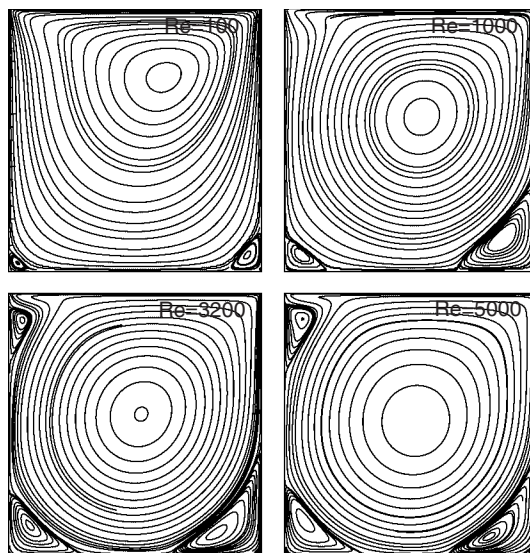


Figure 9. Streamlines for the driven cavity flow problem on a  $257 \times 257$  grid.

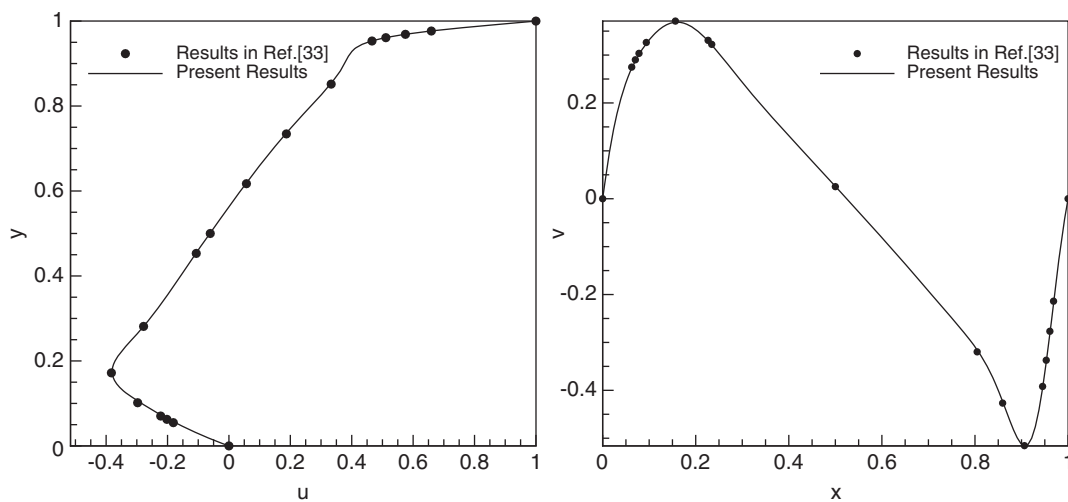


Figure 10. Comparison of  $u$ - and  $v$ -velocity components for  $Re=1000$ .

the order of accuracy, the boundary condition for the pressure is of Dirichlet type, i.e. it uses the analytic solution. Zero velocity is used on all boundaries except along the top surface, where

$$u(x, 1) = 16(x^4 - 2x^3 + x^2) \quad (23)$$

and there is a space-dependent body force  $b$  in the  $y$ -direction given by

$$b(x, y, Re) = \frac{8}{Re} [24F(x) + 2f'(x)g''(y) + f'''(x)g(y)] - 64[F_2(x)G_1(y) - g(y)g''(y)F_1(x)]$$

where

$$f(x) = x^4 - 2x^3 + x^2$$

$$g(y) = y^4 - y^2$$

$$F(x) = \int f(x) dx$$

$$F_1(x) = f(x)f''(x) - [f'(x)]^2$$

$$F_2(x) = \int f(x)f'(x) dx$$

$$G_1(y) = g(y)g'''(y) - g'(y)g''(y)$$

The fact that  $u(0, 1) = 0$  and  $u(1, 1) = 0$  by Equation (23) alleviates the singularity that exists at the top two corners of the classical lid-driven cavity flow problem.

The exact solution for this problem is

$$u(x, y) = 8f(x)g'(y) \tag{24a}$$

$$v(x, y) = -8f'(x)g(y) \tag{24b}$$

$$p(x, y, Re) = \frac{8}{Re} [F(x)g''(y) + f'(x)g'(y)] + 64F_2(x)(g(y)g''(y) - [g'(y)]^2) \tag{24c}$$

Tables I and II show the grid refinement results and orders of accuracy for the third-order and the fifth-order upwind compact schemes, respectively. The order of accuracy is calculated by the following formula:

$$O_A = \frac{\ln(e_2/e_1)}{\ln 2}$$

where

$$e_1 = \phi_e - \phi_f, \quad e_2 = \phi_e - \phi_c$$

$\phi_e$  stands for the exact solution,  $\phi_f$  the solution on a fine grid, and  $\phi_c$  the solution on a coarse grid with half of grid points of the fine grid in each direction. These tables clearly demonstrate that orders of accuracy for the third-order and the fifth-order upwind compact schemes are approximately 3.0 and 5.0, respectively, as anticipated.

## 6. CONCLUSIONS

We have applied third-order and fifth-order upwind compact finite difference scheme to discretizing the convective terms of the incompressible Navier–Stokes equations. These schemes are implemented in conjunction with the artificial compressibility method, which enables the use of

Table I. Grid refinement study for the modified cavity problem using the third-order scheme.

$Re$	Grid	$L_\infty$ error	$L_\infty$ order	$L_1$ error	$L_1$ order	$L_2$ error	$L_2$ order
100	$11 \times 11$	$3.40 \times 10^{-2}$	—	$9.49 \times 10^{-3}$	—	$1.26 \times 10^{-2}$	—
	$21 \times 21$	$5.25 \times 10^{-3}$	2.86	$1.17 \times 10^{-3}$	3.02	$1.52 \times 10^{-3}$	3.05
	$41 \times 41$	$6.71 \times 10^{-4}$	2.97	$1.42 \times 10^{-4}$	3.04	$1.78 \times 10^{-4}$	3.09
	$81 \times 81$	$8.68 \times 10^{-5}$	2.95	$1.73 \times 10^{-5}$	3.04	$2.14 \times 10^{-5}$	3.06
	$161 \times 161$	$9.95 \times 10^{-6}$	3.12	$2.08 \times 10^{-6}$	3.06	$2.59 \times 10^{-6}$	3.05

Table II. Grid refinement study for the modified cavity problem using the fifth-order scheme.

$Re$	Grid	$L_\infty$ error	$L_\infty$ order	$L_1$ error	$L_1$ order	$L_2$ error	$L_2$ order
100	$11 \times 11$	$7.01 \times 10^{-3}$	—	$1.86 \times 10^{-3}$	—	$2.49 \times 10^{-3}$	—
	$21 \times 21$	$2.41 \times 10^{-4}$	4.86	$6.24 \times 10^{-5}$	4.90	$7.82 \times 10^{-5}$	4.99
	$41 \times 41$	$4.59 \times 10^{-6}$	5.71	$1.24 \times 10^{-6}$	5.65	$1.47 \times 10^{-6}$	5.73
	$81 \times 81$	$1.02 \times 10^{-7}$	5.49	$2.20 \times 10^{-8}$	5.82	$2.60 \times 10^{-8}$	5.82
	$161 \times 161$	$2.55 \times 10^{-9}$	5.32	$4.36 \times 10^{-10}$	5.66	$5.56 \times 10^{-10}$	5.55

flux-difference splitting (FDS). The left-hand side of these compact schemes is a linear combination of split derivatives at two grid points, and its right-hand side involves differences of split fluxes between neighboring points, with each difference being computed by using FDS. The resulting upwind compact schemes as well as their boundary treatments are quite simple. The robustness and accuracy of these schemes have been verified in several 2D benchmark problems. The computed results are in good agreement with the published reference solutions. Extension of the present upwind compact schemes to time-dependent and 3D problems is the subject of ongoing work.

#### ACKNOWLEDGEMENTS

This work was supported by the Natural Science Foundation of China (G10531080, G10729101) and the State Key Program for Developing Basic Sciences (2005CB321703). A. Shah would like to thank COMSAT Institute of Information Technology Islamabad, Pakistan for financial support. We also thank the referees for useful comments and suggestions.

#### REFERENCES

1. Chorin AJ. Numerical solution of the Navier–Stokes equations. *Mathematics of Computation* 1968; **22**: 742–762.
2. Chorin AJ. A numerical method for solving incompressible viscous flow problems. *Journal of Computational Physics* 1967; **2**:12–26.
3. Rogers SE, Kwak D. An upwind differencing scheme for the time-accurate incompressible Navier–Stokes equations. *AIAA Journal* 1990; **28**(2):253–262.
4. Rogers SE, Kwak D. An upwind differencing scheme for the incompressible Navier–Stokes equations. *Applied Numerical Mathematics* 1991; **1**(8):43–64.

5. Choi D, Merkle CL. Application of time-iterative schemes to incompressible flow. *AIAA Journal* 1985; **23**: 1518–1524.
6. Hartwich PM, Hsu CH. An implicit flux-difference splitting scheme for 3D incompressible N–S solutions to leading edge vortex flow. *AIAA Paper 86-1839*, 1986.
7. Briley W, Neerarambam S, Whitfield D. Implicit lower–upper/approximate-factorization schemes for incompressible flows. *Journal of Computational Physics* 1996; **128**:32–42.
8. Yuan L. Comparison of implicit multigrid schemes for three dimensional incompressible flows. *Journal of Computational Physics* 2002; **177**:134–155.
9. Yang JY, Yang SC, Chen YN, Hsu CA. Implicit weighted ENO schemes for three-dimensional incompressible Navier–Stokes equations. *Journal of Computational Physics* 1998; **146**:464–487.
10. Hirsh RS. High order accurate difference solutions of fluid mechanics problems by a compact differencing technique. *Journal of Computational Physics* 1975; **19**:90–109.
11. Lele SK. Compact finite difference schemes with spectral-like resolution. *Journal of Computational Physics* 1992; **103**:16–42.
12. Ekaterinaris JA. High-order accurate numerical solutions of incompressible flows with the artificial compressibility method. *International Journal for Numerical Methods in Fluids* 2004; **45**:1187–1207.
13. Fu DX, Ma YW, Kobayashi T. Nonphysical oscillations in numerical solutions: reason and improvement. *CFD Journal* 1996; **4**(4):427–450.
14. Fu DX, Ma YW. A high order accurate difference scheme for complex flow fields. *Journal of Computational Physics* 1997; **134**:1–15.
15. Deng X, Zhang H. Developing high-order weighted compact nonlinear schemes. *Journal of Computational Physics* 2000; **165**:22–44.
16. Tlstykh AI, Lipavskii MV. On performance of methods with third and fifth-order compact upwind differencing. *Journal of Computational Physics* 1998; **140**:205–232.
17. De AK, Eswaran V. Analysis of a new high resolution upwind compact scheme. *Journal of Computational Physics* 2006; **218**:398–416.
18. Roe PL. Approximate Riemann solvers, parameter vectors, and difference scheme. *Journal of Computational Physics* 1981; **43**:357–372.
19. Shen YQ, Yang GW, Gao Z. High-resolution finite compact difference schemes for hyperbolic conservation laws. *Journal of Computational Physics* 2006; **216**:114–137.
20. Gustafsson B. The convergence rate for difference approximations to mixed initial boundary value problems. *Mathematics of Computation* 1975; **29**:396–406.
21. Visbal MR, Gaitonde DV. On the use of higher-order finite-difference schemes on curvilinear and deforming meshes. *Journal of Computational Physics* 2002; **181**:155–185.
22. Beam R, Warming RF. An implicit scheme for the compressible Navier–Stokes equations. *AIAA Journal* 1978; **16**:393–402.
23. Papanastasiou TC, Georgiou GC, Alexandrou AN. *Viscous Fluid Flow*. CRS Press: Boca Raton, 1999.
24. Soh WY, Goodrich JW. Unsteady solution of incompressible Navier–Stokes equations. *Journal of Computational Physics* 1988; **79**:113–134.
25. Ramshaw JD, Mousseau VA. Accelerated artificial compressibility method for steady-state incompressible flow calculations. *Computers and Fluids* 1990; **18**:361–367.
26. Turkel E, Arnone A. Pseudo-compressibility methods for the incompressible flow equations. *ICASE Report 93-66*, 1993.
27. Kwak D, Chang JLC, Shanks SP, Chakravarthy SR. A three-dimensional incompressible Navier–Stokes flow solver using primitive variables. *AIAA Journal* 1986; **24**:390–396.
28. Kim J, Moin P. Application of a fractional step method to incompressible Navier–Stokes equations. *Journal of Computational Physics* 1985; **59**:308–323.
29. Gartling DK. A test problem for outflow boundary conditions, flow over a backward facing step. *International Journal for Numerical Methods in Fluids* 1990; **11**:953–967.
30. Armaly BF, Durst F, Pereira JCF, Schonung B. Experimental and theoretical investigation of backward facing step flow. *Journal of Fluid Mechanics* 1983; **172**:473–496.
31. Shanka ON, Deshpande MD. Fluid mechanics in the driven cavity. *Annual Review of Fluid Mechanics* 2000; **32**:93–136.
32. Garcia S. The lid-driven square cavity flow from stationary to time periodic and chaotic. *Communications in Computational Physics* 2007; **5**(2):900–932.

33. Ghia U, Ghia KN, Shin CT. High  $Re$  solutions for incompressible Navier–Stokes equations. *Journal of Computational Physics* 1983; **49**:387–411.
34. Shih TM, Tan CH, Hwang BC. Effects of grid staggering on numerical scheme. *International Journal for Numerical Methods in Fluids* 1989; **9**:193–212.
35. Pereira JMC, Kobayashi MH, Pereira JCF. A fourth-order-accurate finite volume compact method for the incompressible Navier–Stokes solutions. *Journal of Computational Physics* 2001; **167**:217–243.